Magnetic functionalization of ZnO nanoparticles surfaces via optically generated methyl radicals

D. Marin, G. Gerbaud, O. Margeat, F. Ziarelli, F. Ferrer, O. Ouari, A. Campos, S. Bertaina, Adrien Savoyant

Magnetic functionalization of ZnO nanoparticles surfaces via optically generated methyl radicals

D. Marin,[1] G. Gerbaud,[2] O. Margeat,[3] F. Ziarelli,[4] F. Ferrer,[4] O. Ouari,[4] A. Campos,[5] S. Bertaina,[1] and A. Savoyant[1]

[1)] *Aix-Marseille Université, CNRS, IM2NP UMR 7334, 13397 Marseille Cedex 20, France*

[2)] *Aix Marseille Université, CNRS, Laboratoire de Bioénergétique et Ingénierie des Protéines (UMR7281), IMM, IM2B, Marseille, France*

[3)] *Aix Marseille Université, UMR CNRS 7325, CINaM, Marseille 13288, France*

[4)] *Aix Marseille Univ., CNRS, ICR UMR 7273, 13397 Marseille, France*

[5)] *Aix Marseille Univ, CNRS, Centrale Marseille, FSCM (FR1739),CP2M, 13397 Marseille, France*

(Dated: 20 April 2023)

The combination of nuclear and electron magnetic resonance techniques, in pulse and continuous wave regimes, are used to unravel the nature and features of the light-induced magnetic state arising at the surface of chemically prepared zinc oxide nanoparticles (NPs) occurring under 120 K when subjected to a sub band gap (405 nm) laser excitation. It is shown that the four-line structure observed around $g \sim 2.00$ in the *as-grown* samples (beside the usual core-defect signal at $g \sim 1.96$) arises from surface-located methyl radicals ($^{\bullet}CH_3$), originating from the acetate capped ZnO molecules. By functionalizing the *as-grown* zinc oxide NPs with deuterated sodium-acetate, the $^{\bullet}CH_3$ EPR signal is replaced by trideuteromethyl ($^{\bullet}CD_3$). For $^{\bullet}CH_3$, $^{\bullet}CD_3$ and core-defect signals, an electron spin echo is detected below ∼100 K, allowing for the spin-lattice and spin-spin relaxation-time measurements for each of them. Advanced pulse-EPR techniques reveal the protons or deuterons spin-echo modulation for both radicals, and give access to small unresolved superhyperfine couplings between adjacent $^{\bullet}CH_3$. In addition, electron double resonance techniques show that some correlations exist between the different EPR transitions of $^{\bullet}CH_3$. These correlations are discussed as possibly arising from cross-relaxation phenomena between different rotational states of radicals.

PACS numbers: 31.30.Gs, 32.30.Dx, 32.80.-t 76.30.-v, 76.70.Dx
Keywords: Nanoparticles, ZnO, methyl radical, EPR, double resonance

I. INTRODUCTION

Controlling the physical and chemical surface properties of semiconducting nanoparticles (NPs) is a key point for future nanotechnologies, taking advantage of their high surface-to-volume ratio, of their tunable electronic properties, and of their often-encountered photocatalytic activity. Within a magnetic-application perspective, new surface magnetic states can occur in these nanosized systems, the monitoring of which possibly leading to the realization of nanometric spin-switches, i.e to strongly-localized and monitorable magnetization, with potential application in quantum computing or small magnetic memories and sensors. Such monitorable (by optical or electrical excitation) surface quantum states ultimately arise from a fine balance between chemical and physical interactions of the NPs, highly depending on their growth and stabilization/passivation mechanisms, which is particularly true regarding polar crystals.
Zinc oxide (ZnO) NPs are perhaps the most representative example of such polar nanocrystals[1], hosting intrinsic and extrinsic paramagnetic defects as well[2,3]. When grown by wet chemically based methods, the ZnO NPs are susceptible to be passivated by surrounding organic molecules originating from the solvent, the precursor(s) or the reactants. These surface molecules can survive after drying and washing the NPs and can constitute a stable chemical shell, adding interesting surface magnetic properties to the NPs system[4].

Almost two decades ago, an interesting light-induced (by UV light) paramagnetic signal was detected by pulse electron paramagnetic resonance in ZnO nanocrystals(EPR)[5,6]. This four-line structure (2.4 mT spacing) has been assigned to some ionized Na impurities by these authors, on the basis of weakly resolved ENDOR experiment and the presence of NaOH reactant. However, replacing NaOH by LiOH to obtain Li doping, these authors still observe the same four-line structure, so that its Na origin has remained questionable.
Recently, the same light-induced (violet, 405 nm) signal has been independently detected in a previous work in wet chemically prepared ZnO NPs[7,8], without any intentional presence of Na, and tentatively attributed to bound surface exciton in the high spin-state $S = 2$ with axial anisotropy.

The aim of this paper is to elucidate the nature of this

light-induced signal, generated by illumination at an approximatively 400 nm wavelength threshold for temperature lesser than 120 K, and to demonstrate its potentiality for spin-dynamics based technologies. It is proved by means of EPR techniques and nuclear cross-polarization magic angle spinning (CP-MAS) experiment, performed on *as grown* and *deuterated* samples, that none of the previous assignments are correct, and that this light-induced signal arise in fact from a photo-generated methyl radical ($^{\bullet}CH_3$), itself originating from surface-located passivating acetate precursors. The $^{\bullet}CH_3$ radical gives rise to the four observed EPR transitions, resulting from hyperfine interactions between the unpaired electron in the carbon p_z orbital and the three adjacent protons. This radical is certainly the most archetypal example of small molecular rotor, showing quantum effects at low temperature, when rotation is hindered by a 3-fold potential barrier[9–11]. The coupling between the rotational and nuclear-spin degrees of freedom result in a fully symmetric blocked state of $\mathcal{A}$-type followed by a first excited rotational state of $\mathcal{E}$-type, both belonging to the C_3 point group. The transition between the free and the hindered rotation regimes is detected *via* a change in the intensity ratio of the EPR lines, interpreted as a change in the $\mathcal{A}$ and $\mathcal{E}$ rotational-states population.
Here, these radicals are photo-generated on the ZnO NPs surface, where they benefit from the excitonic properties of these latter, resulting in an interesting organic/inorganic nanosized system. Focusing on the electronic aspect of polarization, the longitudinal (T_1) and transverse (T_2) relaxation times are measured for the unpaired electron spin of $^{\bullet}CH_3$ and for the inner core-defect ($g \sim 1.96$), showing profoundly different dynamics of these two spin systems. The HYSCORES pulse-EPR technique reveals a superhyperfine coupling ($a = 2.72$ MHz) between two adjacent $^{\bullet}CH_3$ radicals. For these surface-adsorbed $^{\bullet}CH_3$, the electron double resonance (ELDOR) technique demonstrates correlation between the different EPR transitions.

II. EXPERIMENTAL

ZnO NPs were prepared following Pacholski *et al.* method[23] . In a first solution, 2.0694 g of Zinc acetate $Zn(Ac)_2$ (Aldrich Chemicals 99.99 %) were solubilized in 105 ml of methanol and 0.625 ml of distilled water. A second solution with 1.1236 g of potassium hydroxide KOH (Aldrich Chemicals 99.99 %) and 57.5 ml of methanol was added dropwise at 60°C under magnetic stirring. After 3h 15, the solution was removed from the thermal bath and submitted to centrifugation during 12 min at 7800rpm. The precipitate was washed with methanol and centrifuged once more. The white solid was dried in an oven at 100°C and referred to as the *as grown* sample.
For the surface functionalization procedure, 5 mg of Sodium acetate-d3 (Aldrich Chemicals 99.99 %) was added to 50 mg of *as grown* ZnO and 2ml of methanol. The solution was centrifuged and the supernatant discarded before adding again the functionalizing component and solvent to the remaining precipitate. This process was repeated 3 times, finally giving the solid referred as *deuterated sample*.
In order to check the independence of the presented results on the solvent (methanol) and catalyst (KOH), other growths with ethanol solvent and NaOH catalyst have been performed, leading to the same EPR spectra.

SEM imaging was performed with a Gemini500 ultra-high resolution field emission electron microscope equipped with an inlens secondary electron (SE) detector, ideal for displaying surface structures. SE images were acquired at a low accelerating voltage (2 kV) to enhance topographic contrast. The NPs have size distribution around 15 nm ± 5 nm effective diameter (Supp. Mat. Sec. I). The TEM imaging was carried out using a FEI TITAN 80–300 electron microscope equipped with an image aberration corrector. The TEM acceleration voltage was 200 kV. The high degree of crystallinity of the NPs is proved by TEM imaging onto a representative small NP, showing the periodic atomic arrangement (Supp. Mat. Sec. I).

The solid-state ^{13}C spectra were obtained on a Bruker Avance-400 MHz NMR spectrometer (magnetic field 9.4 T) using a double channel Bruker probe. About 10 mg of sample was placed in zirconium dioxide rotor of 4 mm outer diameter and spun at a Magic Angle Spinning rate of 10 kHz. The ^1H-^{13}C CPMAS technique[12] was applied with a ramped ^1H-pulse starting at 100% power and decreasing until 50% during the contact time (2ms) in order to circumvent Hartmann-Hahn mismatches. To obtain a good signal-to-noise ratio in ^{13}C CPMAS experiment 15 K scans were accumulated using a delay of 2.2 s. The ^{13}C chemical shifts were referenced to tetramethyl silane and calibrated with glycine carbonyl signal, set at 176.03 ppm.

The cw- EPR experiments have been performed at X-band (9.39 GHz) on a Bruker EMX spectrometer equipped with a standard TE_{102} cavity allowing for external optical excitation. The 85 K temperature equilibrium has been reached with liquid-nitrogen flux and Intelligent Temperature Controller (Oxford, ITC 503). The attenuation A is related to the MW power P by $A = 10\log(P_0/P)$, where P_0 is the maximal MW power. The time evolution study of the L_2 line has been performed on the same powder divided into three tubes, each one filled with different gas (Ar, H_2 and air, respectively), and then definitely sealed by flame. Then, the EPR spectrum has been recorded every week and every two weeks during 220 days in the same conditions (85 K, 15 dB attenuation). Between these measurements the tubes were kept in dark condition at room temperature. Before each measurement, the NPs powders have been subjected to ultrasonic agitation in order to reduce NPs agregation.

X band (9.73 GHz) pulsed-EPR experiments were carried out on a Bruker Elexsys E580 spectrometer equipped with a standard dielectric ring resonator (ER4118X-MD5) and an optical helium flow cryostat (Oxford CF935O) allowing for external optical excitation. Temperature was reached with a closed cycle He Stinger system from Bruker and controlled by a Mercury controller from Oxford. The microwave pulses were amplified with a 1 kW TWT which gives a typical $\pi/2$ pulse of 16ns. HYSCORE measurements were performed at a temperature of 20K with a conventional two-dimensional (2D) four-pulse sequence ($\pi/2$–τ–$\pi/2$–t_1–π–t_2–$\pi/2$–τ–echo). HYSCORE experiments were recorded with a τ delay of 136 ns and a 32 ns detector gate, centered at the maximum of the echo signal, at a repetition rate of 2000 Hz. In all EPR experiments, the dried NPs powders have been optically excited via the solid state laser beam OBIS Coherent LX serie 405 nm at 30 mW optical power, focused on the sample within the EPR cavity.

III. RESULTS

A. Cw-EPR and CP-MAS experiments

The cw-EPR experiments under dark and 405 nm illumination conditions are presented in figure 1. In dark conditions no significant EPR signals are observed above the noise level, although some very weak trace of core-defect signal ($g \sim 1.96$) may exist in some samples. At an illumination threshold of about 400 nm (~ 3 eV), the core-defect signal ($g = 1.964$)[18–21] and the 4-lines structure ($g = 2.005$) simultaneously appear, indicating they are certainly generated by the same quantum of optical excitation. Substantially below the ZnO band gap energy (3.4 eV), this excitation threshold points to the involvement of a strongly bound exciton, or (equivalently) to some localized point-defect ionization.

The generated 4-lines structure (L_1 to L_4) has magnetic field spacing of 2.3 mT and an intensity ratio close to 1:3:3:1, which corresponds to the hyperfine coupling of the free-rotating methyl radical[13] as shown in the simulation displayed in Fig.1-a. The line widths are 0.25±0.01 mT (L_1, L_4) and 0.28±0.01 mT (L_2, L_3). After illumination removal, these lines undergo a slow bi-exponential decay at 85 K[8], and practically no decay under 60 K.

In order to confirm the methyl radical origin and the surface location of this 4-line structure, an after-growth washing with deuterated sodium-acetate ($Na(D\text{-}Ac)_2$) has been performed (see Sec. II). The resulting powder leads to the EPR spectrum of Fig. 1-c and -d. While the 4-lines structure has practically disappeared and has been replaced by a 7-lines structure with shortest spacing, the core-defect signal has not been affected. This confirms that the latter indeed arise from the bulk part of the NPs, not affected by their surface modifications, whereas the former is clearly surface-located.

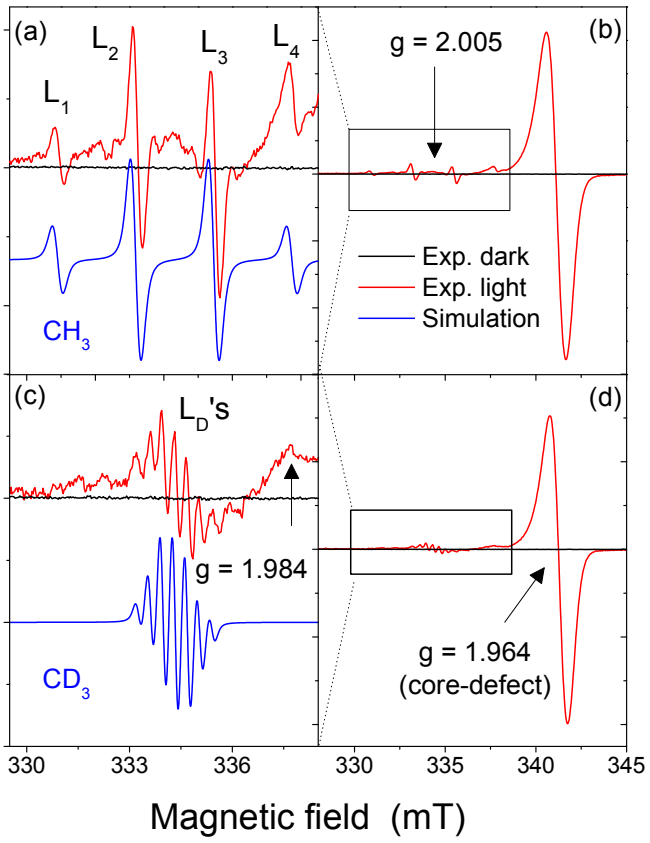

FIG. 1: EPR spectra of ZnO NPs powder at 85 K under dark (black) and 405 nm illumination (red) conditions at 85 K. (a) and (b) show the as grown NPs sample, (c) and (d) the deuterated sample. Left column displays magnification of the surface signal for each case. In blue, the simulations for CH_3 and CD_3 radicals.

The new 7-lines structure exactly corresponds to that of a $^{\bullet}CD_3$ radical, with 0.35 mT spacing due to the hyperfine coupling between the unpaired electron and the three deuterons[13]. The width of the L_D's lines are 0.15±0.03 mT.

In the *as grown* sample the L_4 intensity is substantially greater than that of L_1, suggesting the presence of an underlying line. This is confirmed with the *deuterated* sample, the spectrum of which displaying this isolated line at $g \simeq 1.984$ (Fig. 1). This value is exactly in the middle between the core-defect and the $^{\bullet}CH_3$ or $^{\bullet}CD_3$ gravity center, so that the line can be attributed to some coupling between these two kinds of centers. This intermediate line has been observed and discussed in Ref.[15], where the Q-band frequency allows for the separation of each group of lines.

The stability of the studied photo-generated EPR signals over time and gaseous environment has been established by periodically performing the same experiment on the L_2 and core-defect lines, for an identical NPs powder divided in three EPR quartz tubes filled

respectively with H_2, Ar and air and then sealed. The results are shown in figure 2, displaying notable intensity variability due to the fact that it is not possible to illuminate exactly the same NPs quantity from one measurement to another. Nevertheless, there is clear trends indicating that the core-defect signal intensity has not changed over time, while the L_2 has gained a factor of 5 to 7 during this time. In Air and argon atmosphere the signal's increase can be considered to be the same, while in H_2 this increase is slightly weaker. This is again consistent with a bulk origin of the core-defect, while the $^{\bullet}CH_3$ signal is located on the surface, which undergoes a slow equilibration after growth in favor of a methyl radical signal enhancement. Quite interestingly, this equilibration of the surface appears to be globally independent of the gaseous environment, at least for the 3 gas under study, pointing to the high stability of this magnetic state over time and external conditions.

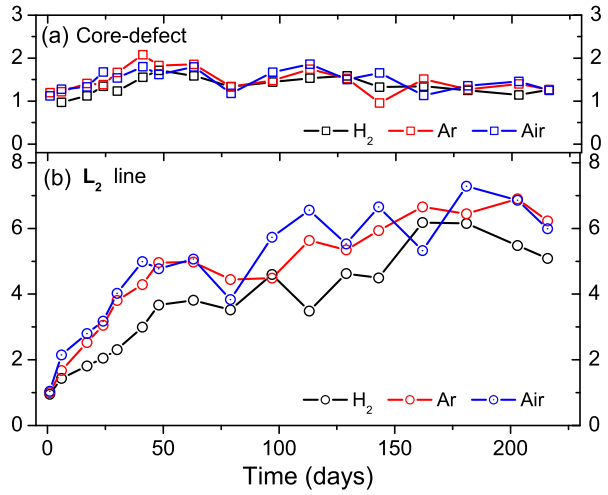

FIG. 2: Time evolution of (a) the core-defect and (b) the L_2 line intensity of CH_3 recorded at 85 K for different gaseous environments.

Aside of these cw-EPR experiment, the *as-grown* and the *deuterated* samples have been studied by the ^{1}H-^{13}C cross polarization solid-state NMR spectroscopy (CPMAS)[12] at room temperature and in dark condition, allowing for the signature detection of the ^{13}C isotope coupled to specific hydrogen protons. The main features of the *as-grown* sample consist of two signals at 23.6 and 180.5 ppm (Fig. 3), corresponding respectively to the methyl group and to the carboxylate group of an acetate molecule[14]. This measurement indicates the notable presence of these molecules at the surface of the ZnO NPs, certainly originating from the Zn-(acetate)$_2$ precursor, and involved in the passivation of the ZnO polar surface during growth.
Regarding the *deuterated* sample, the same two signals are still present, with the methyl signal intensity at

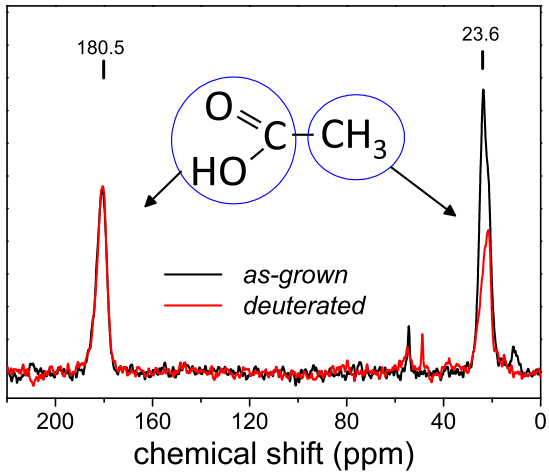

FIG. 3: ^{1}H–^{13}C NMR cross polarization performed on the *as-grown* and the *deuterated* samples, showing the part corresponding to the methyl and carboxylate subgroup of the acetate molecule.

23.6 ppm divided by two in intensity, while the carboxylate group remains unchanged, which indicates the partial deuteration by CD_3COOH acetates. Combined with cw-EPR data, it definitely proves that the four-lines structure arises from $^{\bullet}CH_3$ radicals and, moreover, that these $^{\bullet}CH_3$ radicals originate from those residual acetate precursors located at the NPs surface.

B. Pulse-EPR experiments

The electron-spin polarization dynamics of the surface radicals have been probed by pulse-EPR experiments for the *as grown* and *deuterated* powders. A clear Hann echo[24] is detected up to 120 K (Supp. Mat. Sec. II), at the fields and frequency corresponding to the resonance of the L_1 to L_4 lines for the as-grown sample, and at the center of the 7-lines group for the deuterated sample.

The spin-spin relaxation is probed by the two pulses ESEEM sequence (recorded at 20 K), showing the magnetization decay and possible nuclear modulation. The results are shown in figure 4 for the *as-grown* and *deuterated* samples, in both time and frequency domains. The left panels display the decay of the echo intensity as the τ time between $\pi/2$ and π pulses is incremented, providing information about the phase memory time T_m. This time dependence is fitted by a exponential decay with variable exponent, whose parameters for each line are summarized in Table I of supplementary material section III. Time constants of about 2500 and 1500 ns are deduced, respectively for the $m_I = \pm 3/2$ ($L_{1,4}$) and $m_I = \pm 1/2$ ($L_{2,3}$) lines of CH_3, and around 2000 ns for the gravity center of CD_3.

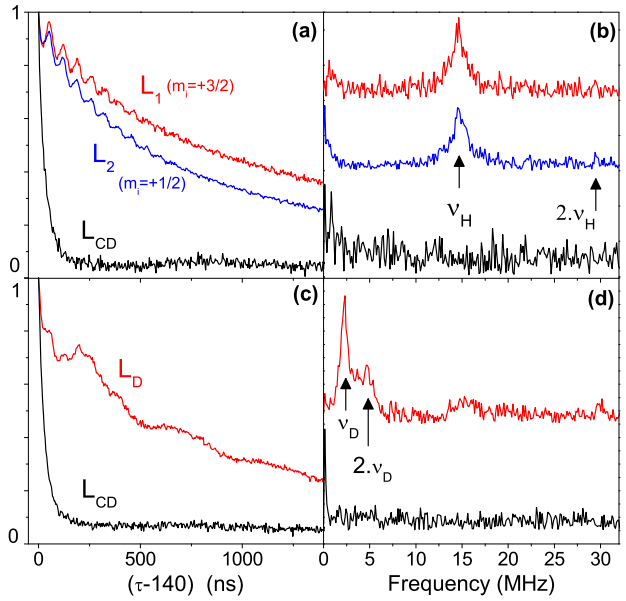

FIG. 4: (a) Two-pulses ESEEM data recorded at $T = 20$ K on the various lines of the as *grown sample* and (b) FFT transforms after biexponential substraction of ESEEM data. (c) and (d), the same for the *deuterated* sample.

In both samples, the core-defects display very short phase memory time ($\sim$ 70 ns) without nuclear modulation, as compared to that of the electron spin of the surface $^{\bullet}CH_3$ and $^{\bullet}CD_3$. It is to be noted that this result is consistent with a recent work giving the global transverse relaxation time T_2 for core-defect (deduced from the cw-EPR line width) to be of about 30-50 ns[16], logically shorter than T_m because of the additional inhomogeneous defocusing contribution to the global decay. The absence of ESEEM modulation for the core-defect signal indicates the absence of protons in the vicinity of this paramagnetic center, suggesting an intrinsic point defect origin.

These ESEEM data display the modulation of the spin-echo intensity during its decay, clearly visible on the left panels of figure 4. In order to quantify more precisely these oscillations, a Fourier transform is performed (after bi-exponential decay substraction and apodization) on the ESEEM data, resulting in the right panel of figure 4. For the *as-grown* sample, the single proton Larmor frequency $\nu_H = 14.6$ MHz at $B = 346.0$ mT is detected, while for the deuterated sample the deuteron frequency $\nu_D = 2.32$ MHz and its double $2.\nu_D = 4.64$ MHz are at $B = 347.0$ mT. The zero-frequency component of these Fourier transform correspond to some remaining constant baseline after the biexponential substraction. Aside, at the core-defect line of the *as-grown* sample, a weak peak at 0.85 MHz could be attributed to the ^{67}Zn isotope ($\nu_{Zn} = 0.91$ MHz), consistently with a bulk ZnO location.

The ESEEM signals only exists if there is a quadrupole nuclear interaction or if a hyperfine anisotropy is present, the latter case being at work here. For the *as-grown* sample, considering an excitation width at half maximum of about 20 MHz (corresponding to the inverse of the 32 ns π-pulse length), the observed nuclear modulation cannot be related to the inner $^{\bullet}CH_3$ hyperfine coupling ($A = 66$ MHz), because at least two nuclear transitions must be simultaneously excited for the oscillations to be observed. Rather, the observed modulation must be due to some weak (super)hyperfine coupling ($a < 2\omega_H$), unresolved in the cw-EPR experiment, so that both of these nuclear transitions can be simultaneously excited by the pulse.

This assumption is supported by the HYSCORE experiments which allow for resolving very weak couplings by means of a two-dimensional 3-pulses ESEEM involving the incrementation of two times τ_1 and τ_2. The two-dimensional Fourier transform shows some satellite peaks around the main nuclear frequency ($\nu_H = 14.8$ MHz), resulting from weak superhyperfine interaction with protons characterized by an isotropic constant $a = 2.72$ MHz ~ 0.1 mT unresolved in the cw regime (Fig. 5-a).

In the *deuterated* sample (Fig. 5-b), the proton frequency has disappeared and the deuteron frequency is visible at $\nu_D = 2.4$ MHz. Satellite peaks around the diagonal occur in the left panel which indicates a strong coupling regime ($A_D > 2\nu_D$). These peaks are spaced by $2\nu_D$ and centered around the $A_D/2$ value, which has been verified by simulation with *Easyspin*[25] for a 1/2 electronic spin and three $I = 1$ nuclear spins. These results indicate that in the *deuterated* sample all protons are removed from the vicinity of the $^{\bullet}CD_3$ radicals, which strongly suggests that in the *as-grown* sample, all the detected protons are those of $^{\bullet}CH_3$ radicals. Thus, the superhyperfine coupling (a) in the *as-grown* can be attributed to ($^{\bullet}CH_3$)–($^{\bullet}CH_3$) interaction.

In order to probe the correlation between the different transitions of $^{\bullet}CH_3$, the electron-electron double resonance technics ELDOR has been used. It consists in exciting the system with a first $\pi/2$ selective pumping pulse (128 ns) with variable frequency (f_p), to wait a time $5T_2^m$ for achieving a total in-plane dephasing, and then to apply the classical spin echo sequence $\pi/2 - \pi$ at the field and frequency (f_t) corresponding to one of the four CH_3 transitions, the target transition. The frequency detuning between the two frequencies is denoted by $\Delta f = f_p - f_t$. At high detuning, the first pulse does not correspond to any transition, neither allowed or forbidden, and has thus no influence on the following echo whose intensity is then maximal. At exactly zero detuning ($\Delta f = 0$), the first pumping pulse completely saturates the target transition (equalizing its levels population) so that the following detecting

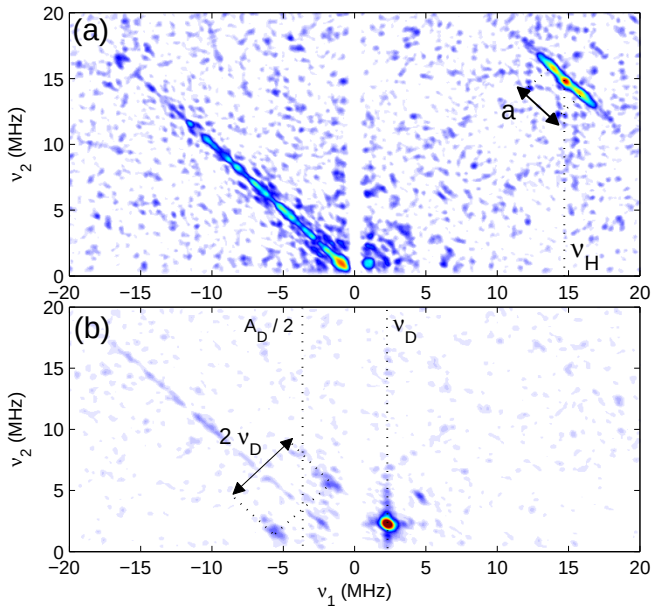

FIG. 5: HYSCORE measurements recorded at $T = 20$ K (a) on the L_2 lines (346.0 mT) and (b) on the gravity center of the L_D's (347.0 mT), showing respectively weak ($a < 2\nu_H$) and strong ($A_D > 2\nu_D$) coupling cases.

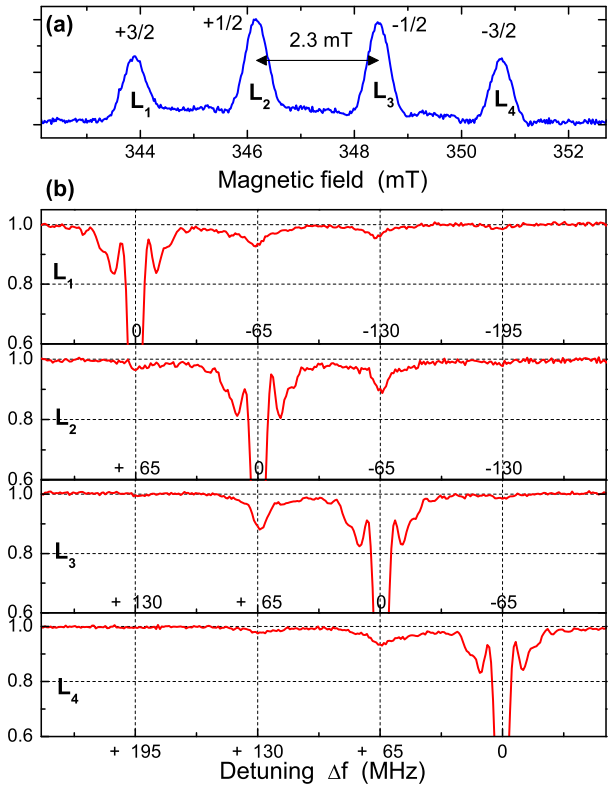

FIG. 6: (a) Field-sweep pulse EPR spectrum of as grown ZnO NPs, showing the total m_I prohection of each transition. (b) ELDOR spectra recorded at L_1, L_2, L_3, L_4 field and primary frequency $f_1 = 9.738$ GHz as function of detuning $\Delta f = f_2 - f_1$. All data recorded at $T = 20$ K.

sequence gives no echo intensity (hole burning).
The interesting phenomenon occurs when the detuning equals the value of another close transition. In this case, the pumping pulse saturates this close transition, and the decrease in the adjacent transitions then must arise from a correlation between them. In a high-spin system ($S > 1/2$), this echo-intensity lowering is commonly due to a depopulating effect occurring when the two transitions of different $|m_S|$ share a common level. In an ELDOR-detected NMR (EDNMR) experiment[34,35], the correlation is also due to a depopulation effect of a common level shared by two transitions, but with one EPR-allowed transition ($\Delta m_S = \pm 1$, $\Delta m_I = 0$, the target transition) and one EPR-forbidden transition ($\Delta m_S = \pm 1$, $\Delta m_I = \pm 1$, the pumped transition), thus requiring a very long pumping pulse. Here, none of these possibilities is relevant because the correlations occur between the *allowed* transitions of a 1/2 electronic spin.

In figure 6-a, the field-sweep echo intensity is plotted, showing the four $^{\bullet}CH_3$ transitions with ratio intensity clearly different from 1:3:3:1 at $T = 20$ K. In figure 6-b the ELDOR spectra are shown, repeated for each transition. At zero detuning, the echo intensity falls to zero, while at multiple of 65 MHz (= 2.3 mT) a weak intensity decrease (∼10%) is observed, pointing to the transitions correlation. Possible explanations for these observed correlations are discussed in the following section.
The satellite holes around the central hole (at zero detuning) are proved to be inversely proportional to the pumping pulse length, so that they are simply the Fourier transform in the frequency domain of the rectangular 128 ns pumping pulse, i.e the wings of a cardinal sinus.

IV. DISCUSSION

The system under study constitutes an interesting example of coupling between organic and inorganic subsystems, with core and surface defects displaying paramagnetic response in a nanosized system, activatable by visible light. While the NPs shell is a complex semi-amorphous zone potentially containing several type of molecules, the massive presence of acetates molecules certainly participate in the passivation of the ideally positively charged surface at low temperature by releasing a proton toward the negatively charged surface and leaving a negatively charged acetate at the opposite surface (Fig. 7-b, -c).

The results of section III A show that, in the *as grown* sample, the photo-generated four EPR lines (L_1 to L_4) actually arise from methyl radicals, originating from those growth-residual acetates located on surface. The long-time evolution measurements point to a slow equilibration/reorganization of the NPs surface, after growth and drying, which favors the generation of the methyl radicals by the optical excitation. Moreover, these excited surface radicals appears to be mostly unaffected by the gaseous environment (at least for air, Ag and H_2 gases), and largely stable and reproducible over several months.
In the *deuterated* sample, the $^{\bullet}CH_3$ radicals EPR signal has practically disappeared, replaced by the $^{\bullet}CD_3$ signal, whereas only a fraction of the whole acetates have been actually replaced by deuterated acetates, as shown by the cw-EPR and CP-MAS experiments.

Beside of these $^{\bullet}CH_3$ or $^{\bullet}CD_3$ radicals, the commonly observed core-defect signal in ZnO nanostructures at $g = 1.96$ is simultaneously generated at the same excitation wavelength, $\lambda \sim 400$ nm. Indeed, this optical threshold is basically related to the core-defect[16], so that the radical generation must be seen as a *consequence* of the core-defect ionization, and not the reverse. This core-defect signal is always present under dark condition (without illumination) in ZnO nanostructures grown by high-temperature (HT) methods. For low-temperature (LT) growths, either the core-defect signal exists in dark condition and no $^{\bullet}CH_3$ signal is created by illumination, or no signals are present at all in dark condition and core-defect and $^{\bullet}CH_3$ are simultaneously created by illumination (present case).

This situation can be understood by attributing the core-defect signal to some rather deep intrinsic acceptor defect (most probably a zinc vacancy[26]), either neutral (X^0, non-magnetic) or negatively charged (X^-, paramagnetic) depending on its electrostatic environment. The central point is to consider that an ideal bare finite-portion of ZnO has positively and negatively fictive surface charges at the (Zn^{2+})- and (O^{2-})-terminated surface, respectively, which in turn generate a constant internal depolarizing electrical field. The corresponding non-uniform potential drives the system off thermodynamical equilibrium so that this latter must, in a way or another, capture or generate electrical charges in order to passivate the surfaces and to reach equilibrium. Without the presence of organic molecules (HT growth case), the passivation can only be achieved by ionizing those X defects localized near the (Zn^{2+})-terminated surface toward the X^- state, resulting in a core-defect signal ($g = 1.96$) in dark condition. When organic molecules are present (LT growth case), they can participate in the surface passivation, thus reducing the number of ionized core-defect in dark condition.
In the present case, it can be assumed that the massive presence of negatively charged acetates is sufficient for passivating the positive surface, so that almost all the neighboring core-defects are in their neutral non magnetic state X^0 and no EPR signal is observed in dark condition (Fig. 7-b). When subjected to ∼400 nm illumination, the core-defects undergo an ionization toward X^- state, thus liberating a hole able to reach the surface where it can suppress the negative charge of the acetate ion, resulting in the catalytic dissociation of its methyl group. In other words, under illumination, the passivation source of the positive surface switches from acetate ions to near-surface ionized intrinsic core-defects. This scenario is supported by the annealing of ZnO NPs which removes the organic surface molecules (Supp. mat. Sec. V), resulting in an intense X^- signal observed in dark conditions and which is practically not modified by illumination.
The dissociation of the acetate molecule at the heart of the aboved-discussed scenario is a kind of sub-band gap photo-Kolbe reaction[27–29], in which the photo-generated hole comes from a point defect rather than from the valence band.

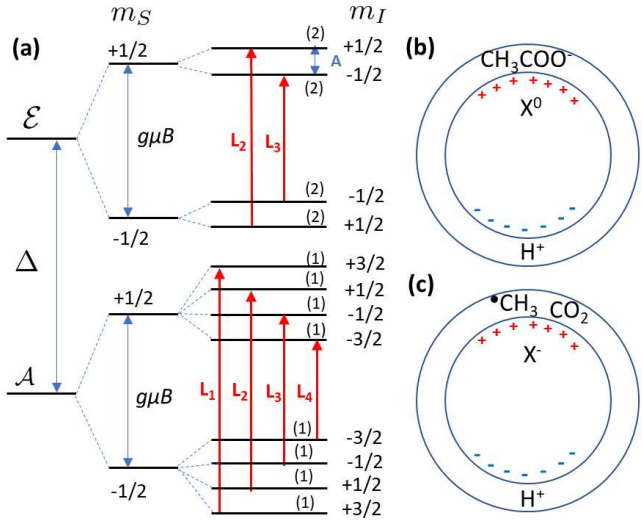

FIG. 7: (a) Levels diagram of the $^{\bullet}CH_3$ radical. Electron spin (m_S) and total nuclear spin (m_I) projection are indicated for each level, as well as their degeneracy in brackets. Core-shell model of the passivated ZnO NP showing the two polar surface, the X^0 core-defect and the Ac^- adsorbed molecule before illumination (b) and the X^- core-defect ($g = 1.96$) and $^{\bullet}CH_3$ radical after illumination (c).

Regarding the physical interest for this system, the photo-generated $^{\bullet}CH_3$ radical provides an easily excitable unpaired electron spin, with a relatively high protonic degeneracy. This methyl radical is widely studied, as part of a more complex molecule, embed in inert-gases matrix, trapped in porous material (zeolite), or adsorbed at other organic or inorganic materials

surface[30–33]. Here, the coupling to ZnO NPs furnishes the possibility for exciting a quasi-stable surface magnetic state in the visible region (below the band gap 3.4 eV). The idea underlying this work is to take advantage of this surface-located photo-generated radical on an inorganic NPs, susceptible to be individually manipulated or spread onto addressable nanosized array, contrary to commonly observed radicals or point defects randomly distributed in a solid bulk matrix.
The detection of the electron spin echo at each of the $^{\bullet}CH_3$ lines indicates the presence of magnetic inhomogeneities within. The cw-EPR line width of about 0.3 mT corresponds to a global transverse time decay of ~ 100 ns, below the spectrometer dead time (140 ns) so that the field-induced decay (FID) cannot be directly detected. Rather, the spin-echo decay measurement with increasing τ time between pulses gives access to the homogenous phase memory time T_2^m, whose values for $L_{1,4}$ ($\sim$ 2500 ns) and $L_{2,3}$ ($\sim$ 1500 ns) correspond to a maximal homogeneous line widths of 0.014 mT and 0.024 mT, respectively. In practice it can be retained that the homogeneous decay divides the initial $^{\bullet}CH_3$ transverse magnetization by two in two µs. For the *deuterated* sample, an intermediate T_2^m is found ($\sim$ 2000 ns), certainly because in this case all the seven lines with different m_I projections are simultaneously excited. For the core-defect a very short T_2^m is found ($\sim$ 70 ns) in both samples, from which it can be stated that $T_2^m \sim T_2$, i.e the homogeneous and inhomogeneous line widths must be almost identical. This fact, together with the absence of proton modulation for the core-defect, implies that these X^- centers must be surrounded by an important electron spin density, consistently with a location not far from the positive polar-surface hosting the radicals (see Fig. 7-b,-c).

Concerning the $^{\bullet}CH_3$ signal, the modulation of the echo intensity decay by the surrounding protons (the ESEEM signal) indicates a weak anisotropic hyperfine coupling, partially responsible (together with field inhomogeneity and orientation averaging) for the inhomogeneous line width. The HYSCORE measurement on the *as-grown* sample gives the isotropic part of this super-hyperfine coupling (a = 2.72 MHz $\sim$ 0.1 mT), consistently with the above considerations about homogeneous and inhomogeneous line widths. Moreover, these HYSCORE measurements on the *deuterated sample* shows that when surface acetates are replaced by deuterated acetates, even the proton modulation (i.e the diagonal peak) disappears, which strongly suggests that this superhyperfine interaction arises from the coupling between two methyl radicals, i.e between the electron of a given $^{\bullet}CH_3$ and the protons of another adjacent one. Such a coupling between two photo-generated radicals on an inorganic NP can be of great interest for Q-bit technologies[4]. Moreover, a kind of J-coupling between the surface radical and the ionized core-defect is detected at the intermediate g-value (1.984)[15].

The electron spin longitudinal relaxation time T_1 for the core-defect, the $^{\bullet}CH_3$ and the $^{\bullet}CD_3$ radicals has also been measured in the *as-grown* and *deuterated* samples. The results, presented in the supplementary material section IV, give values of $\sim$40 µs (the shortest component) for all transitions of $^{\bullet}CH_3$, $\sim$30 µs for $^{\bullet}CD_3$, and 140 µs for the core defect. Contrary to the measured transverse dephasing T_2^m times, T_1 is longer for the core-defect. These longitudinal times constant (the T_1's) are related to the thermal stability of a given polarized spin, a crucial feature for potential applications, and constitute the ultimate limit for T_2^m, when all spin-spin interactions are suppressed.
In addition, the Rabi oscillations for the three spin systems have been measured (Supp. Mat. Sec. VI), which show that all the observed transitions are those of a 1/2 electronic spin.

An interesting point in the photo-generated $^{\bullet}CH_3$ radical on ZnO NPs system is that each of the four possible transitions can be separately excited by a selective pulse, thus exciting only a subspace of the total spin set, namely that corresponding to a given total nuclear spin projection m_I $(-3/2, -1/2, +1/2, +3/2)$. At low temperature ($\sim 20\ K$), the change in the intensity ratio from 1:3:3:1 to 1:X:X:1 ($X \sim 1.4$, see Fig. 6-a) indicates a change in the two lowest rotational states population ($\mathcal{A}$ and $\mathcal{E}$), because $m_I = \pm 3/2$ can only exist within the ground $\mathcal{A}$ level, whereas $m_I = \pm 1/2$ can in both $\mathcal{A}$ and $\mathcal{E}$ levels (see Fig. 7-a). For a free-rotating methyl radical, the maximal energy separation between the two lowest rotational states is $\Delta = 5.22\ cm^{-1} = 7.5$ K, which is lowered by the threefold potential barrier[36]. The methyl rotation is then not free anymore, but hindered by this substantial potential barrier resulting from various interactions with environment.
Regarding the transitions correlation observed in the ELDOR experiment when Δf is a multiple of $A = 66$ MHz (Fig. 6-b), its origin is likely to be a cross-relaxation phenomena between different rotational states of single radical or between two adjacent ones[37]. More insight into these interesting quantum tunneling relaxation mechanism would require a detailed temperature study in single and double resonance experiments. Our preliminary measurement show a clear departure from the Curie law of the $^{\bullet}CH_3$ cw-EPR intensity both at high and low temperature, with an *intensity* × *temperature* maximum around 25-30 K.
A full temperature study would also be of great interest in order to get insight into the NPs polar surface passivation, where interplay between surface chemical and bulk intrinsic defect mechanisms appear to occur in this work. In particular, the role of electron donnors (e.g interstitial hydrogen, oxygen vacancy, zinc interstitial) in the positive-surface passivation as function of temperature would be worth to study by some contactless conductivity measurements, in the spirit of Ref. 38. Depending on

the donnor level position below the conduction band, the impurities electrons would be localized near the positive surface at high temperature or at their donnor site at low temperature, switching from electronic to chemical passivation as the temperature is lowered.

V. CONCLUSION

The presence of optically-generated methyl and trideuteromethyl radicals at the surface of ZnO NPs, quasi-stable under 120 K, has been established by various magnetic resonance technics. These radicals originate from the acetate surface species, themselves originating from the Zn-acetate precursors, independently of the kind of reactant or solvent. These acetates are involed in the polar surface passivation by releasing a proton toward the negative surface, leaving an Ac^- at the positive surface. This photo-generation of radicals $^\bullet CH_3$ and $^\bullet CD_3$ is enhanced with time after growth, reaching a maximum after approximately 5 months. Basically, the involved mechanism is a kind of photo-Kolbe reaction, in which a photo-excited hole is transferred from a point acceptor defect to the surface Ac^-, resulting in the dissociation of this latter.
The electron spin dynamics has been probed by various pulse EPR technics. Relaxation times are found to be of order of few tens of microseconds for the longitudinal relaxations T_1 and of about two microseconds for the transverse dephasing time T_2^m, for both radicals. In the case of $^\bullet CH_3$ a very weak hyperfine coupling between both of these radicals has been detected by HYSCORE technics, and responsible for the proton modulation of the spin echo intensity. An electron double resonance technics has probed some correlations between the different EPR transitions of $^\bullet CH_3$, tentatively assigned to some cross-relaxation phenomena between different rotational states of the radical.

VI. SUPPLEMENTARY MATERIAL

The supplementary material file contains (I) the SEM and TEM imaging, (II) the spin-echo temperature dependence, (III) the fits data for T_1 and (IV) for T_2^m times, (V) the cw-EPR figure of *as-grown* and *annealed* samples a, and (VI) the Rabi oscillation measurements.

The data that support the findings of this study are openly available in Zenodo at DOI: 10.5281/zenodo.7825018

VII. ACKNOWLEDGEMENT

This work is supported by Agence Nationale de la Recherche (ANR project "SPIMAN", ANR-21-CE09-0027-01). Financial support from the IR INFRANALYTICS FR2054 for conducting the research is gratefully acknowledged. Dr. Michaël Texier is acknowledged for TEM imaging.

[1] I. Ayoub, V. Kumar, R. Abolhassani, R. Sehgal, V. Sharma, R. Sehgal, H. C. Swart, and Y. K. Mishra, *Nanotechnol. Rev.* **11**, 575 (2022). DOI: 10.1515/ntrev-2022-0035
[2] I. Elhamdi, H. Souissia, O. Taktaka, J. Elghoulbc, S. Kammouna, E. Dhahri, and B. F. O. Costad, *RSC Adv.*, 2022, 12, 13074-13086. DOI: 10.1039/D2RA00452F
[3] L. S. Vlasenko, *Appl. Magn. Reson.* **39**, 103 (2010).DOI: 10.1007/s00723-010-0140-1
[4] A. Y. Lee, T. A. Colleran, A. Jain, J. Niklas, B. K. Rugg, T. Mani, O. G. Poluektov, and J. H. Olshansky, *J. Am. Chem. Soc.* **145**, 8, 4372 (2023). DOI: 10.1021/jacs.2c11952
[5] S. B. Orlinskii, J. Schmidt, P. G. Baranov, D. M. Hofmann, C. de Mello Donegá, and A. Meijerink, *Phys. Rev. Lett.* **92**, 047603 (2004) DOI: 10.1103/PhysRevLett.92.047603
[6] S. B. Orlinskii, H. Blok,E. J .J. Groenen, J. Schmidt, P. G. Baranov,C. de Mello Donegá, and A. Meijerink, *Magn. Reson. Chem.* **43** S140-S144 (2005). DOI: 10.1002/mrc.1686
[7] A. Savoyant, M. Rollo, M. Texier, R. E. Adam, S. Bernardini, O. Pilone, O. Margeat, O. Nur, M. Willander and S. Bertaina, *Nanotechnology* **31** (2020) 095707. DOI: 10.1088/1361-6528/ab57f1
[8] A. Savoyant, C. Sebastiao, and O. Margeat, *Phys. Status Solidi RRL* **14**, 2000176 (2020). DOI: 10.1002/pssr.202000176
[9] C. C. Lin and J. D. Swalen, *Rev. Mod. Phys.* **31**, 841 (1959). DOI: 10.1103/RevModPhys.31.841
[10] J. H. Freed, *J. Chem. Phys.* **43**, 1710 (1965). DOI: 10.1063/1.1696995
[11] T. Yamada, K. Komaguchi, M. Shiotani, N. P. Benetis, and A. R. Sørnes, *J. Phys. Chem. A* **103**, 25, 4823 (1999). DOI: 10.1021/jp984716g
[12] J. Schaefer, E. O. R. Stejskal, *J. Am. Chem. Soc.* **98**, 1031 (1976).
[13] J. Turkevich and Y. Fujita, *Science* **152**, 1619 (1966). DOI: 10.1126/science.152.3729.1619
[14] G. C. Levy, R. L. Lichter, and G. L. Nelson, *Carbon-13 Nuclear Magnetic Resonance Spectroscopy*, Wiley (1980).
[15] P. G. Baranov, S. B. Orlinskii, C. de Mello Donegá, *et al.*, *Appl. Magn. Reson.* **39**, 151–183 (2010). DOI: 10.1007/s00723-010-0151-y
[16] H. H. Kim, H. Lee, J. K. Kang, and W. K. Choi, *Ann. Phys. (Berlin)*, 2100382 (2022). DOI: 10.1002/andp.20210038
[17] D. M. Hofmann, A. Hofstaetter, F. Leiter, H. Zhou, F. Henecker, B. K. Meyer, S. B. Orlinskii, J. Schmidt, and P. G. Baranov, *Phys. Rev. Lett.* **88**, 045504 (2002). DOI: 10.1103/PhysRevLett.88.045504
[18] H. Kaftelen, K. Ocakoglu, R. Thomann, S. Tu, S. Weber, and Emre Erdem, *Phys. Rev. B* **86**, 014113 (2012). DOI: 10.1103/PhysRevB.86.014113
[19] E. Erdem, *J. Alloys Compd.* **605**, 34 (2014). DOI: 10.1016/j.jallcom.2014.03.157
[20] S. Repp, S. Weber, and E. Erdem, *J. Phys. Chem. C*, **120**, 43, 25124 (2016). DOI: 10.1021/acs.jpcc.6b09108
[21] A. Savoyant, H. Alnoor, O. Pilone, O. Nur, and M Willander, *Nanotechnology* **28** 285705 (2017). DOI: 10.1088/1361-6528/aa716a/meta
[22] Volodin, A.M., Cherkashin, A.E. ERS spectrum of methyl radicals on ZnO surface. React Kinet Catal Lett 18, 243–246 (1982). DOI: 10.1007/BF02065172
[23] C. Pacholski, A. Kornowski, and H. Weller, . Angewandte Chemie International Edition, Wiley Online Library, v. 41, n. 7, p.1188–1191, 2002.
[24] E. L. Hahn, *Phys. Rev. B* **80**, 580 (1950). DOI: 10.1103/PhysRev.80.580
[25] S. Stoll and A. Schweiger, *J. Magn. Reson.* **178**, 42 (2006). DOI: 10.1016/j.jmr.2005.08.013
[26] S. Nadupalli , S. Repp , S. Weber and E. Erdem, *Nanoscale* **13**, 9160 (2016). DOI: 10.1021/acs.jpcc.6b09108

[27]S. Sato, *J. Phys. Chem.* **87**, 3531 (1983). DOI: 10.1021/j100241a034
[28]M. Schmitt, S. Kuhn, M. Wotocek, and R. Hempelmann, *Z. Phys. Chem.* **225**, 297 (2011). DOI:10.1524/zpch.2011.0050
[29]M. Schmitt, *Macromol. Chem. Phys.* **213**, 1953 (2012). DOI: 10.1002/macp.201200309
[30]T. B. Freedman, E. R. Nixon, *Spectroc. Acta A* **28**, 1375 (1972). DOI: 10.1016/0584-8539(76)80266-8
[31]D. K. Murray, J. W. Chang, and James F. Haw, *J. Am. Chem. Soc.* **115**, 11, 4732 (1993) DOI: 10.1021/ja00064a037
[32]Q. Guo, C. Xu, W Yang, Z. Ren, Z. Ma, D. Dai, T. K. Minton, and X. Yang, *J. Phys. Chem. C* **117**, 10, 5293 (2013). DOI: 10.1021/jp401613s
[33]G. Jeschke, *Appl. Magn. Reson.* **53**, 635 (2022). DOI: 10.1007/s00723-021-01375-6
[34]D. Goldfarb, *eMagRes* **6**, 101 (2017). DOI:10.1002/9780470034590.emrstm1516
[35]N. Cox, A. Nalepa, W. Lubitz, and A. Savitsky, *J. Mag. Res.* **280**, 63 (2017). DOI: 10.1016/j.jmr.2017.04.006
[36]M. M. Somoza and J. Friedrich, *Fiz. Nizk. Temp.* **32**, 1345 (2006). DOI: 10.1063/1.23890087
[37]J. R. Harbridge., S. S. Eaton, G. R. Eaton, *J. Magn. Reson.* **159**, 195 (2002). DOI: 10.1016/s1090-7807(02)00013-7
[38]D. Savchenko, A. Vasin, O. Kuz, I. Verovsky, A. Prokhorov, A. Nazarov, J. Lančok, and E. Kalabukhova, *Sci. Rep.* **10**, 17347 (2020). DOI: 10.1038/s41598-020-74449-3